

1 **Seasonal Variation of Total Column Formaldehyde, Nitrogen Dioxide, and Ozone Over Various Pandora**
2 **Spectrometer Sites with a Comparison of OMI and Diurnally Varying DSCOVR-EPIC Satellite Data**

3

4

5

6

Jay Herman^{1,2} and Jianping Mao^{2,3}

7

8

9

10

11

12

13

14

15

16

17

18

19

20

21 ¹GESTAR II University of Maryland Baltimore County, Baltimore, Maryland USA

22 1000 Hilltop Cir, Baltimore, MD 21250

23 ²NASA Goddard Space Flight Center, 8800 Greenbelt Road, Greenbelt, MD 20771, USA

24 Correspondence: Jay Herman (herman@umbc.edu)

25 ³College of Computer, Mathematical and Natural Sciences, University of Maryland, College Park, MD
26 20740, USA

27

28

29

30

31 Abstract

32 Observations of trace gases, O₃, HCHO, and NO₂, and their seasonal dependence can be observed using
 33 satellite and ground-based data from the Ozone Monitoring Instrument (OMI) satellite and Pandora
 34 ground-based instruments. Both operate with spectrometers that have similar characteristics in
 35 wavelength range and spectral resolution that enable them to retrieve total column amounts of
 36 formaldehyde (TCHCHO), and nitrogen dioxide (TCNO₂), and total column ozone (TCO). The polar
 37 orbiting OMI observes at 13:30 ± 0:25 local time plus an occasional second side-scan point 90 minutes
 38 later at mid-latitudes. The ground-based Pandora spectrometer system observes the direct sun all day
 39 with a temporal resolution of 2 minutes. At most sites, Pandora data show a strong seasonal
 40 dependence for TCO and TCHCHO and less seasonal dependence for TCNO₂. Use of a low pass filter
 41 Lowess(3-months) can reveal the seasonal dependence of TCNO₂ for both OMI and Pandora at mid-
 42 latitude sites usually correlated with seasonal heating using natural gas or oil. Compared to Pandora,
 43 OMI underestimates the amount of NO₂ air-pollution that occurs during most days, since the OMI
 44 TCNO₂ retrieval is around 13:30± 0:25 local time, which tends to occur near the frequent minimum of
 45 the daily TCNO₂ time series. Even when Pandora data are restricted to between 13:00 and 14:00 hours
 46 local time OMI retrieves less TCNO₂ than Pandora over urban sites because of OMI's large field of view.
 47 The seasonal behavior of TCHCHO is mostly caused by the release of HCHO precursors from plant
 48 growth and emissions from lakes that peak in the summer as observed by Pandora and OMI. Long-term
 49 averages show that OMI TCHCHO usually has the same seasonal dependence but differs in magnitude
 50 from the amount measured by Pandora and is frequently larger. Comparisons of OMI total column NO₂
 51 and HCHO with Pandora daily time series show both agreement and disagreement at various sites and
 52 days. For ozone, daily time dependent comparisons of OMI TCO with those retrieved by Pandora show
 53 good agreement in most cases. Additional diurnal comparisons are shown of Pandora TCO with hourly
 54 retrievals during a day from EPIC (Earth Polychromatic Imaging Camera) spacecraft instrument orbiting
 55 the Earth-Sun Lagrange point L₁.

56 1.0 Introduction

57 Formaldehyde, HCHO, is ubiquitous in the atmosphere and as with other VOCs (Volatile Organic
 58 Compounds) are derived from natural and anthropogenic sources, such as plants, animals, biomass
 59 burning, fossil fuel combustion, and industrial processes (Zhang et al., 2019; Morfopoulos et al., 2021).
 60 Formaldehyde is mainly produced from the oxidation of VOCs such as isoprene, methane, and
 61 anthropogenic emissions (Wittrock, 2006). Formaldehyde can also be directly emitted from some
 62 sources, such as vehicle exhaust, tobacco smoke, building materials, and wood burning affecting
 63 pollution levels both indoors and outdoors. The majority of gaseous and atmospheric formaldehyde
 64 derives from microbial and plant decomposition (Peng et al., 2022). HCHO concentrations in the first few
 65 kilometers of the atmosphere vary depending on the location, time of day, season, and meteorological
 66 conditions. Some of the factors that influence total atmospheric column amounts of HCHO are:

- 67 • **Solar radiation:** Formaldehyde is photolyzed by solar ultraviolet radiation (Nussbaumer et al., 2021)
 68 and broken down into smaller molecules and radicals. The photolysis rate of formaldehyde depends
 69 on the solar zenith angle, the cloud cover, and the atmospheric composition. Generally,
 70 formaldehyde photolysis is faster in the summer and during midday.
- 71 • **Temperature:** The thermal decomposition rate of formaldehyde increases with temperature, which
 72 means it is faster in warmer regions and seasons.
- 73 • **Humidity:** Formaldehyde reacts with water vapor in the atmosphere, forming formic acid and
 74 hydroxyl radicals. The reaction rate of formaldehyde with water vapor depends on the relative

75 humidity, which varies with the temperature and the precipitation. Generally, formaldehyde
76 reaction with water vapor is faster in humid regions and seasons.
77

78 The largest sources of NO_2 are obtained from fossil fuel burning from various types of automobiles truck
79 emissions and power generation followed by industrial processes and oil and gas production (Van der A,
80 2008; Stavrou et al. 2020). Additional sources are soils with natural vegetation, oceans, agriculture
81 with the use of nitrogen rich fertilizers, forest fires, and lightning. In populated areas requiring winter
82 heating, anthropogenic sources of lower tropospheric NO_2 are larger than natural sources. Nitrogen
83 oxides play a major role in atmospheric chemistry and the production and destruction of ozone in both
84 the troposphere and stratosphere. In the boundary layer high concentrations of both HCHO (Kim et al.,
85 2011) and NO_2 (Faustini et al., 2014) are health hazards for humans.

86
87 TCHCHO, TCNO₂ and TCO in the atmosphere are typically measured by satellite and ground-based
88 instruments.

- 89 • Satellite: The Ozone Monitoring Instrument (OMI) is a satellite sensor launched in July 2004 that
90 measures HCHO, NO_2 , O_3 , and other atmospheric constituents from space (Levelt et al. 2018).
91 Detailed descriptions of the OMI instrument are given in Levelt et al. (2006) and Dobber et al.
92 (2006). Briefly, OMI is a side scanning spectrometer instrument (270 to 500 nm in steps of 0.5 nm)
93 with a nadir spatial resolution of $13 \times 24 \text{ km}^2$. OMI data can be used to monitor their global
94 distribution and long-term trends, and to investigate the role of NO_2 and HCHO in atmospheric
95 chemistry and air quality (Lamsal et al., 2014; 2015; Boeke et al., 2011). For ozone, DSCOVR (Deep
96 Space Climate Observatory), located at the Earth-Sun gravitational balance Lagrange point L_1 ,
97 contains a filter-based instrument EPIC (Earth Polychromatic Imaging Camera) capable of obtaining
98 TCO once per hour (90 minutes in Northern hemisphere winter) simultaneously for the entire sunlit
99 globe as the Earth rotates (Herman et al., 2018) with nadir resolution of $18 \times 18 \text{ km}^2$.
- 100 • Ground-based Spectrometer: The Pandora spectrometer system forms a worldwide network of over
101 150 currently working direct-sun observing instruments that match atmospheric observations with
102 known laboratory spectra of HCHO, NO_2 , and O_3 to obtain the total vertical column above the
103 Pandora instrument every 2 minutes from multiple co-added spectra. Pandora uses a single-grating
104 spectrometer and a charge-coupled device (CCD) 2048×64 -pixel detector to record the direct-sun
105 spectra in the ultraviolet and visible wavelength range, 280 – 525 nm with an oversampled 0.6 nm
106 spectral resolution. The retrieval algorithm is based on a spectral fitting technique to retrieve the
107 slant column densities of O_3 , HCHO, NO_2 and other gases, and then convert them to vertical column
108 densities using geometric air mass factors appropriate for direct-sun observations. Pandora
109 spectrometers have been deployed in various field campaigns and locations to monitor the spatial
110 and temporal variability of TCHCHO and TCNO₂ to validate and improve the satellite observations of
111 TCHCHO (Herman et al., 2009, Tzortziou et al., 2015, Spinei et al., 2018).

112
113 This study will examine the seasonal cycles of total column NO_2 , HCHO, and O_3 seen by the Pandora
114 instruments by examining multi-year (2021 – 2024) time series for seasonal and daily behavior at various
115 sites and will compare with observations made from the OMI satellite overpass measurements based
116 on OMI gridded $0.25^\circ \times 0.25^\circ$ data for the Pandora sites. Pandora ozone measurements will be
117 additionally compared to hourly data obtained from EPIC. All of the Pandora data used in this study are
118 after the upgrade of the instruments to eliminate internal sources of HCHO (Spinei, et al., 2021). Part of
119 this study (TCNO₂ and TCO) is an extension of Herman et al. (2019) using Pandora data (2012 – 2017)

120 before the internal upgrade. A difference is that Pandora TCO is now compared with hourly TCO
 121 retrieved by DSCOVER-EPIC. Table 1 shows a list of Pandora sites used in this study.

122

Table 1 List of 30 Pandora locations used in this study and figure of appearance

	Pandora Number	Pandora location name	Lat (deg)	Long (deg)	Alt(m)
1	Pan 180 Fig.1,2	Bronx, New York USA	40.868	-73.878	31
2	Pan 64 Fig.3	New Haven, Connecticut USA	41.301	-72.903	4
3	Pan 190 Fig.4	Bangkok, Indonesia	13.785	100.540	6
4	Pan 182 Fig.5	Tel Aviv, Israel	32.113	34.806	8
5	Pan 159 Fig. 6	Wakkerstroom, South Africa	-27.349	30.144	18
6	Pan 20 Fig.7	Busan, Korea	50.798	4.358	107
7	Pan 145 Fig.10	Toronto-Scarborough, Canada	43.784	-79.187	14
8	Pan 134 Fig. 12	Bristol, Pa, USA	40.107	-74.882	10
9	Pan 204 Fig. 12	Boulder, Co USA	40.038	-105.242	161
10	Pan 106 Fig.12,A2	Innsbruck, Austria	47.264	11.385	616
11	Pan 117 Fig.12	Rome Italy	41.907	12.5158	75
12	Pan 193 Fig.12	Tsukuba, Japan	36.066	140.124	51
13	Pan 140 Fig.13,A2	Washington, DC USA	38.922	-77.012	6
14	Pan 166 Fig.7,A2	Philadelphia, Pa USA	39.992	-75.081	6
15	Pan 238 Fig.14	Granada	37.164	-3.605	7
16	Pan 240 Fig. 14	Thessaloniki, Greece	40.6336	22.9561	60
17	Pan 66 Fig.15	Huntsville Alabama USA	34.725	-86.646	22
18	Pan 156 Fig.15	Hampton, Virginia USA	37.020	-76.337	19
19	Pan 39 Figs.12,15	Dearborn, Michigan USA	42.307	-83.149	18
20	Pan 101 Fig.A1	Izania, Spain	28.309	-16.499	24
21	Pan 119 Fig.A1,A2	Athens, Greece	37.998	23.775	130
22	Pan 124 Fig.A1	Comodoro Rivadavia	-45.7833	-67.45	46
23	Pan 131 Fig. A1	Palau	7.3420	134.4722	23
24	Pan 135 Fig.A1,A2	CCNY Manhattan NY USA	40.815	-73.951	34
25	Pan 142 Fig.A1	Mexico City, Mexico	19.326	-99.176	2280
26	Pan 146 Fig.A1	Yokosuka, Japan	35.321	139.651	5
27	Pan 147 Fig.A1	Detroit, Mi USA	42.303	-83.107	178
28	Pan 150 Fig.A1,A2	Ulsan, Korea	35.575	129.190	38
29	Pan 154 Fig.A1	Salt Lake City Ut, USA	40.766	-75,081	1455
30	Pan 162 Fig.A1	Brussels, Belgium	50.798	4.358	107

123

124 2.0 Examples of Seasonal and Daily Variation of HCHO and NO₂

125 Worldwide Pandora total column data can be downloaded from the Austrian Pandonia project website
 126 <https://data.pandonia-global-network.org/> or from a US NASA backup site updated every week.
 127 https://avdc.gsfc.nasa.gov/pub/DSCOVER/Pandora/DATA_02/. Of interest for this study are the Level-2
 128 (L2) time series ASCII files for direct-sun observations. For example, the Bronx New York City files for
 129 Pandora instrument 180 for TCNO2 data are in Pandora180s1_BronxNY_L2_rnvs3p1-8.txt, TCHCHO in
 130 Pandora180s1_BronxNY_L2_rfus5p1-8.txt, and TCO data in Pandora180s1_BronxNY_L2_rout2p1-8.txt
 131 with the 9 bold characters identifying the file contents. **This naming convention applies to all Pandora**
 132 **sites.**

133 The Pandora data are arranged in irregular columns that are identified in the metadata header for each
 134 file. In the current version, column 1 contains the GMT date and time for each measurement and
 135 column 39 contains measured column density in moles m⁻² (multiply by 6.02214076x10²³/2.6867 x10²⁰ =

136 2241.4638 to convert to DU where $1 \text{ DU} = 2.6867 \times 10^{20} \text{ molecules m}^{-2}$). Pandora data also contain
 137 measurements of water vapor, and SO_2 total column amounts in different files.

138 The original OMI data has a resolution of $13 \times 24 \text{ km}^2$ at the center of the OMI side-to-side scan. The
 139 overpass OMI data is based on the latest gridded version with $0.25^\circ \times 0.25^\circ$ pixel resolution
 140 (midlatitudes approximately $30 \times 30 \text{ km}^2$). The closest OMI pixel to each Pandora site within 50 km
 141 is used for time matched comparisons. Long-term time series use all available Pandora data
 142 between 07:00 and 17:00 filtered for data quality (values with large RMS errors and with negative
 143 values are removed). Diurnal comparisons with OMI on specified days use Pandora minute-by-
 144 minute data that are nearly continuous suggesting that Pandora is observing the direct sun under
 145 clear-sky conditions. Clouds cause some scatter in consecutive data points.

146 Figure 1 shows the seasonal and daily variation of total column HCHO (TCHCHO) and NO_2 (TCNO2) in
 147 Bronx, New York. The daily data for 1 week in July and September shows the range of values for both
 148 weekdays and weekends. When all the Bronx TCHCHO data are plotted as an aggregate for 3 years, there
 149 is a strong seasonal pattern with a maximum in July and a minimum near the end of December. The
 150 summer seasonal dependence of TCHCO is consistent with the surface HCHO values observed by the
 151 ground-based Air-Quality System AQS (Wang et al., 2022). For TCNO2, there is a weaker seasonal
 152 pattern as shown in the Lowess(0.033) fit to the data (Cleveland, 1979; Cleveland and Devlin, 1988) with
 153 moderate maxima in January-February, since the sources of NO_2 are largely from the nearly constant
 154 flow of cars and trucks. The parameter 0.033 is the fraction of the time-series data included in the local
 155 least squares estimate, or about 1 month for Pan 180.

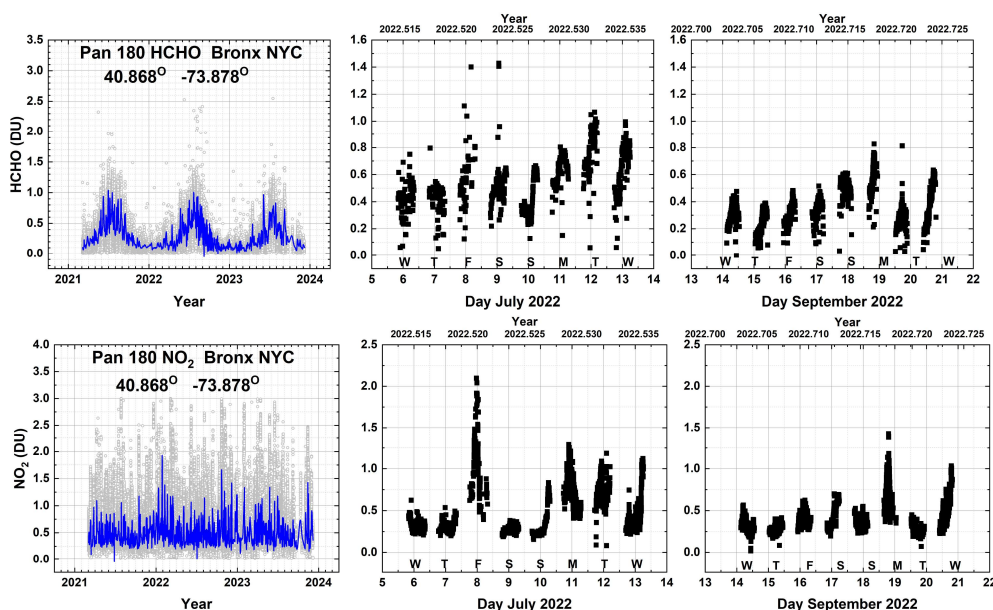


Fig. 01 Seasonal and daily behavior of HCHO and NO_2 from Pan 180 located in the Bronx, NYC at 40.868°N , -73.878°W . The blue lines are a Lowess(0.033) fit to the data (light grey), which is approximately a 1-month local least-squares average. The Local principal investigator for Pan 180 is Dr. Luke Valin.

156

157 Figure 2 shows the daily average of Pandora data obtained from diurnal variation of TCHCHO and TCNO₂
 158 from 09:00 to 15:00 local standard time (GMT – 5). The primary emission sources of atmospheric HCHO

159 include direct emissions of HCHO precursors from vegetation and lakes, primarily through the release of
 160 biogenic volatile organic compounds such as isoprene and terpenes from vegetation, the soil, biomass
 161 burning, and decaying plant and animal matter. This is consistent with the Bronx location that is
 162 adjacent to a large, vegetated park with a small lake near Fordham University. The same TCHCHO
 163 seasonal dependence and magnitude occurs when the Pandora sampling is restricted to 13:00 to 14:00
 164 local standard time similar to the OMI overpass time.

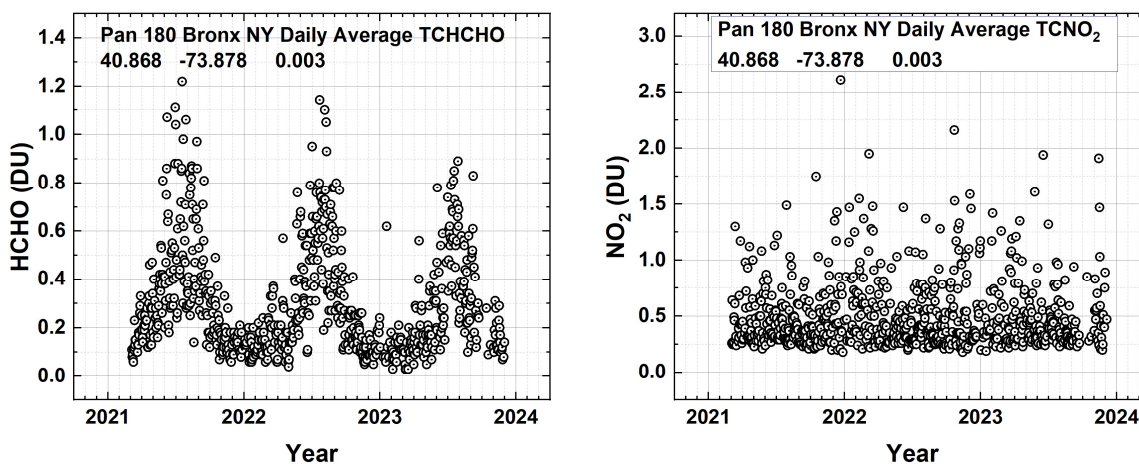


Fig. 02 The daily average seasonal variation of TCHCHO and TCNO₂ in DU over Fordham University in Bronx, New York City from Pandora 180 at 40.868° latitude, -73.878° longitude, and 0.003 km altitude. Each point is a daily average of the data in Fig.1. Local principal investigator: Dr. Luke Valin.

165

166 There are 3 Pandora sites in New York City and one in nearby Bayonne, New Jersey. The NYC sites are in
 167 the Bronx-Fordham University, Manhattan-City College NY (CCNY), Queens-Queens College. All four
 168 successfully measured NO₂ in the period 2021 – 2023. A strong seasonal cycle in TCNO₂ is not seen (Figs.
 169 1 and 2) in the traffic driven production of NO₂ in the Bronx, New York. The mean values of total column
 170 NO₂ (TCNO₂) for each of the 3 New York sites are 0.5 DU while the TCNO₂ for the port city of Bayonne,
 171 NJ is substantially higher at 0.7 DU. None of the four sites show a large seasonal daily average TCNO₂
 172 pattern. For TCHCHO, all four sites show an annual seasonal cycle with three of the sites having a 3-year
 173 average of 0.3 DU except for the Queens site at 0.45 DU. The Queens site may be anomalous because of
 174 many missing points affecting the average.

175 Similar behavior is seen at other sites such as the one from New Haven Connecticut located in a
 176 vegetated area adjacent to two rivers (Fig.3). TCHCHO has a clear summer peak in June – July and a
 177 weak winter TCNO₂ peak in December to January coinciding with the maximum heating season.

178 The seasonal variation of TCHCHO could not be studied prior to the internal upgrade of Pandora after
 179 2019 that was needed because of the release of HCHO from polyoxymethylene (POM-H Delrin) out-
 180 gassing as a function of daytime temperature within the Pandora sun-pointing optical head (Spinei et al.,
 181 2021)

182

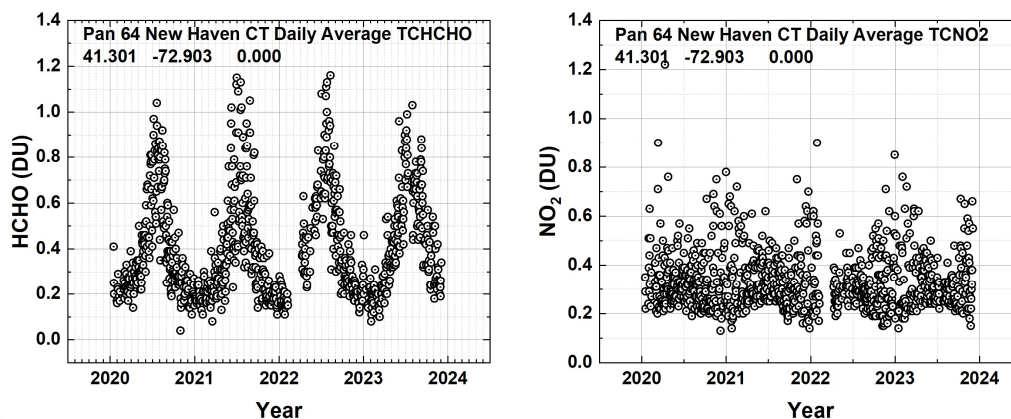


Fig. 03 The seasonal variation of TCHCHO and TCNO2 over New Haven Connecticut from Pandora 64 at 41.301°N latitude and -72.903°W longitude. Each point is a daily average. Local principal investigator: Dr. Nader Abuhassan

183

184 An equatorial Pandora site (Fig. 4) with a sufficiently long data record is located in Bangkok, Indonesia
 185 near a small park and lake. Bangkok has a tropical monsoon climate with three main seasons: hot season
 186 from March to June, rainy season from July to October, and cool season between November and
 187 February. TCHCHO has a seasonal cycle peaking in March – April when the sun is nearly overhead and a
 188 minimum during the rainy season. TCNO2 has a clear seasonal cycle peaking in December – January and
 189 a minimum during the rainy season. Bangkok has a tropical climate with April as the hottest month with
 190 temperatures averaging at 30.5°C (87°F) and the coldest is December at 26°C (79°F).

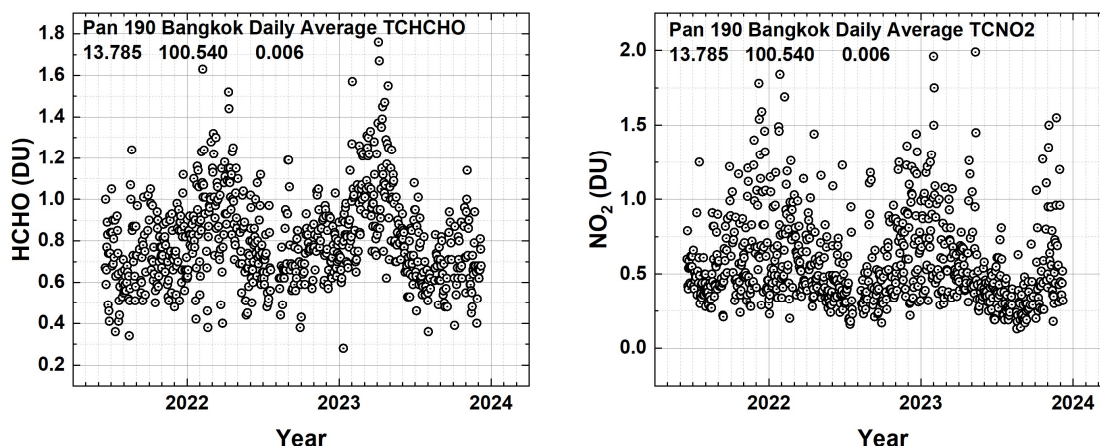


Fig. 04 The seasonal variation of TCHCHO and TCNO2 over equatorial Bangkok Indonesia at 13.785°N and 100.540°E . The local principal investigator is Surassawadee Phoompanit.

191

192 An unusual counter example to the typical TCHCHO seasonal cycle is for the Pandora site located in Tel
 193 Aviv Israel. Tel Aviv has significant amounts of HCHO but does not show seasonal variation in TCHCHO
 194 because of a coastal location in a warm climate even at midlatitudes located at 32.113°N , 34.085°E that
 195 has essentially two seasons, a cool, rainy winter: October – April and a dry, hot summer: May –
 196 September. The result is there is limited seasonal increase in vegetational activity and almost no
 197 seasonal variation in HCHO (Fig. 5). However, TCNO2 shows a clear seasonal increase in the December -

198 January months frequently reaching over 0.5DU. The TCNO₂ seasonality is similar to that of the near-
 199 surface concentrations reported by Boersma et al., (2009). The Pandora instrument 182 is located at Tel
 200 Aviv University about 1 km from a major highway. Tel Aviv has frequent episodes of smog associated
 201 with heavy automobile and truck traffic (Newmark, 2001). Heating and cooling in Tel Aviv are mainly
 202 electrical with the maximum power generation occurring in the summer, suggesting that the winter
 203 TCNO₂ peak is not caused just by electrical power generation from natural gas that emits NO₂.

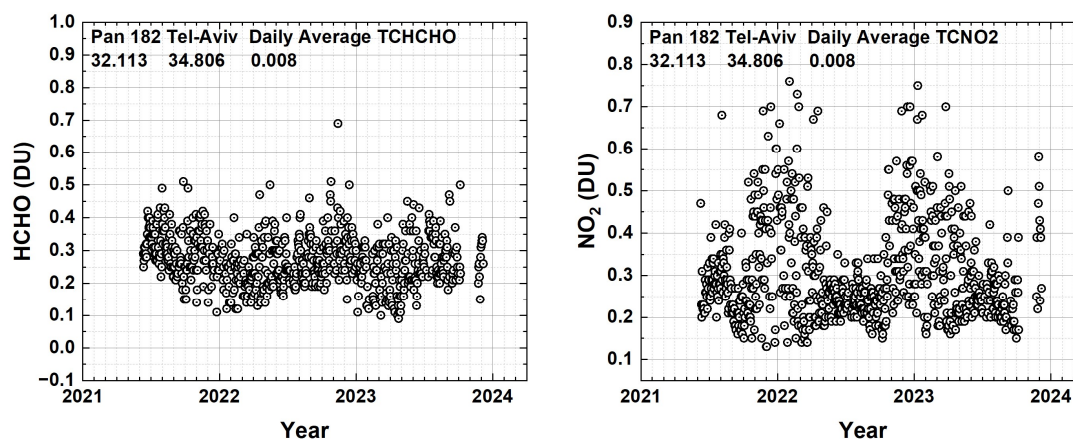


Fig. 05 Seasonal variation in daily average TCHCHO and TCNO₂ in Tel Aviv Israel from Pandora 182 located at 32.113°N, 34.085°E at a height of 8 meters. The local principal investigator for Pan 182 is Dr. Michal Rozenhaimer.

204

205 Finally, a Pandora example from the Southern Hemisphere SH from Wakkerstroom, South Africa located
 206 in a rural area near the ocean a few degrees outside of the equatorial zone at -27.359°S and 30.144°E.

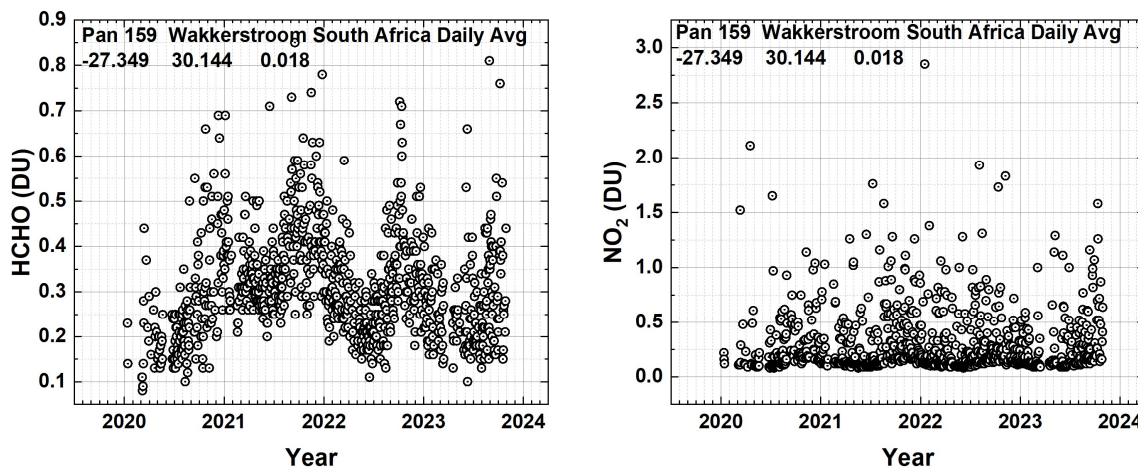


Fig. 06 Seasonal variation in daily average HCHO and NO₂ in Wakkerstroom South Africa from Pandora 159 located at -27.359°S and 30.144°E at a height of 18 m. Local principal investigator: B. Scholes

207

208 As expected, the peak value of TCHCHO occurs near the SH summer in November – December, while
 209 TCNO₂ has no significant seasonal dependence.

210

211 2.1 Comparisons Between Pandora and OMI Retrievals of NO₂ and HCHO

212 In this section three types of comparisons of Pandora with OMI satellite data are considered. First (Fig. 7
213 upper panels), is the TCNO₂ time series consisting of the data record of Pandora and OMI from 2020 –
214 2023. The second (Fig. 7 lower panels) is a low-pass Lowess(3-months) filter of midday TCNO₂ showing
215 the seasonal variation. The third (Fig. 8), looks at a few selected days in May, July, and December and
216 compares typical Pandora clear-sky values with the mid-afternoon OMI overpass at times near 13:30
217 hours equator crossing time. Pandora and OMI data are matched at the same GMT and then converted
218 to local solar time, GMT + Longitude/15. The OMI overpass HCHO and NO₂ data are found at
219 <https://avdc.gsfc.nasa.gov/pub/data/satellite/Aura/OMI/V03/L2OVP/OMHCHO/>.

220 <https://avdc.gsfc.nasa.gov/pub/data/satellite/Aura/OMI/V03/L2OVP/OMNO2/>.

221 Figure 7 (upper 2 panels) illustrates that OMI only captures the mid-day fraction of the daily values of
222 total column NO₂ and fails to detect the extent of the daily pollution at both the Bronx New York City
223 and Busan Korea sites. This is because OMI and other polar orbiting satellites only collect data once per
224 day (occasionally twice per day) at any given location at mid-afternoon, frequently when TCNO₂ is
225 below its daily maximum (Lamsal et al., 2015; Herman et al., 2019). The lower 4 panels of Fig. 7 reveal
226 the seasonal dependence of TCNO₂ at two mid-latitude Northern Hemisphere sites found by using a 3-
227 month low-pass filter Lowess(3 Months) showing that there is an annual TCNO₂ cycle peaking in the
228 winter that corresponds to the natural gas and oil heating use. The Pandora (13:00 to 14:00) values are
229 larger than those from OMI especially at Busan suggesting that the OMI gridded overpass field of view
230 0.25° x 0.25° includes areas of lower NO₂ values over the nearby ocean. In the case of the Bronx, the
231 differences are smaller but also include areas over rivers. Philadelphia Pennsylvania is landlocked but
232 smaller than an OMI gridded footprint so that the OMI field of view contains somewhat less polluted
233 suburbs making the OMI TCNO₂ closer to the Pandora values. The Boulder Colorado Pandora is in a
234 small landlocked city where the OMI field of view extends over sparsely populated regions leading to
235 OMI TCNO₂ lower than Pandora values.

236

237

238

239

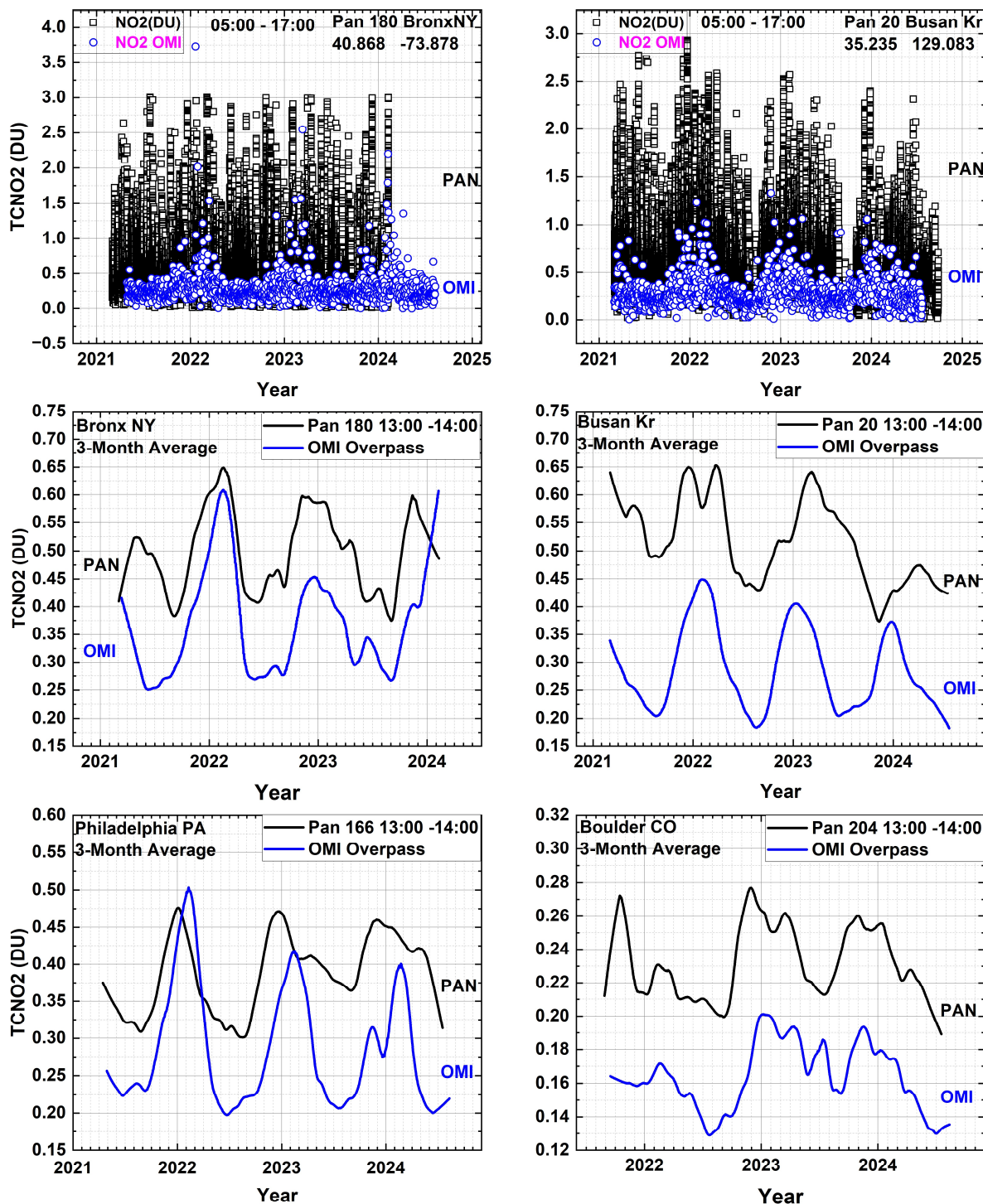


Fig. 07 Upper 2 Panels: Comparison of OMI (approximately 13:30) and Pandora (07:00 – 17:00) total column NO₂ time series in Bronx NY (40.868°N, -73.878°W) and Busan Korea (35.235°N, 129.083°E). Lower 4 Panels: Pandora data for Bronx, Busan, Philadelphia (39.992°N, -75.081°W) and Boulder (40.0375°N, -105.242°W) are averaged between 13:00 – 14:00 hours. Both OMI (blue) and Pandora (black) then have a Lowess(3-month) low-pass filter applied. Local principal investigator for Pan20 is Jae Hwan Kim, for Pan 180 and Pan 166 is Dr. Luke Valin, and for Pan 204 Dr. Nader Abuhassan.

240 Figures 8 and 9 show the diurnal daytime variation for 3 selected days for Pandora retrieved total
 241 column NO₂ and HCHO compared with OMI at the overpass time for both the Bronx in New York City
 242 Busan, Korea and Philadelphia, Pennsylvania. These are typical examples of the highly variable hourly
 243 variation of TCHCHO and TCNO₂ as observed by Pandora on **clear-sky days** at most sites.

244

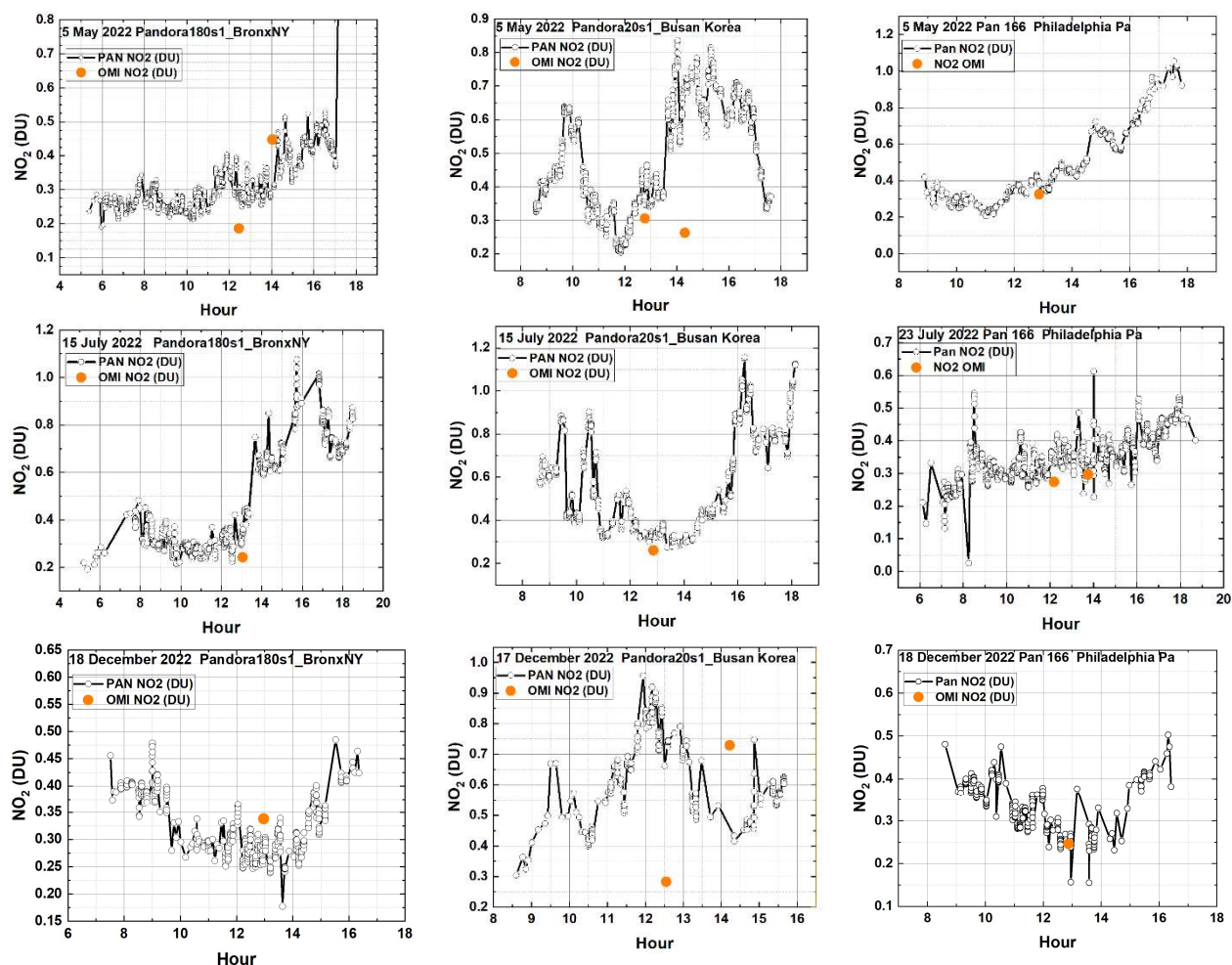


Fig. 08 A comparison between Pandora and OMI (Orange circle) total column NO₂ for 3 locations (Bronx, New York, Busan Korea, Philadelphia, Pennsylvania). The Local principal investigator for Pan 180 and Pan 166 is Dr. Lukas Valin and for Pan 20 is Dr. Jae Hwan Kim.

245

246 The hourly variation of TCHCHO and TCNO₂ on any given day can take on unique shapes depending on
 247 the presence of surface winds, changes in temperature, **and the amount of** sunlight. The variability of
 248 TCNO₂ is also driven by the strength of the sources (automobile exhaust, power generation, industry,
 249 etc.) as well as the meteorological conditions. On some days, there is good agreement (within 10%) but

250 in general the OMI overpass values do not agree with Pandora retrieved values for both TCHCHO and
 251 TCNO₂. In the sample shown in Figures 8 and 9, the cases of agreement are about 70% of the time for
 252 TCNO₂ and 30% for TCHCHO. Also, the OMI TCNO₂ frequently is less than the daily maximum of TCNO₂.

253

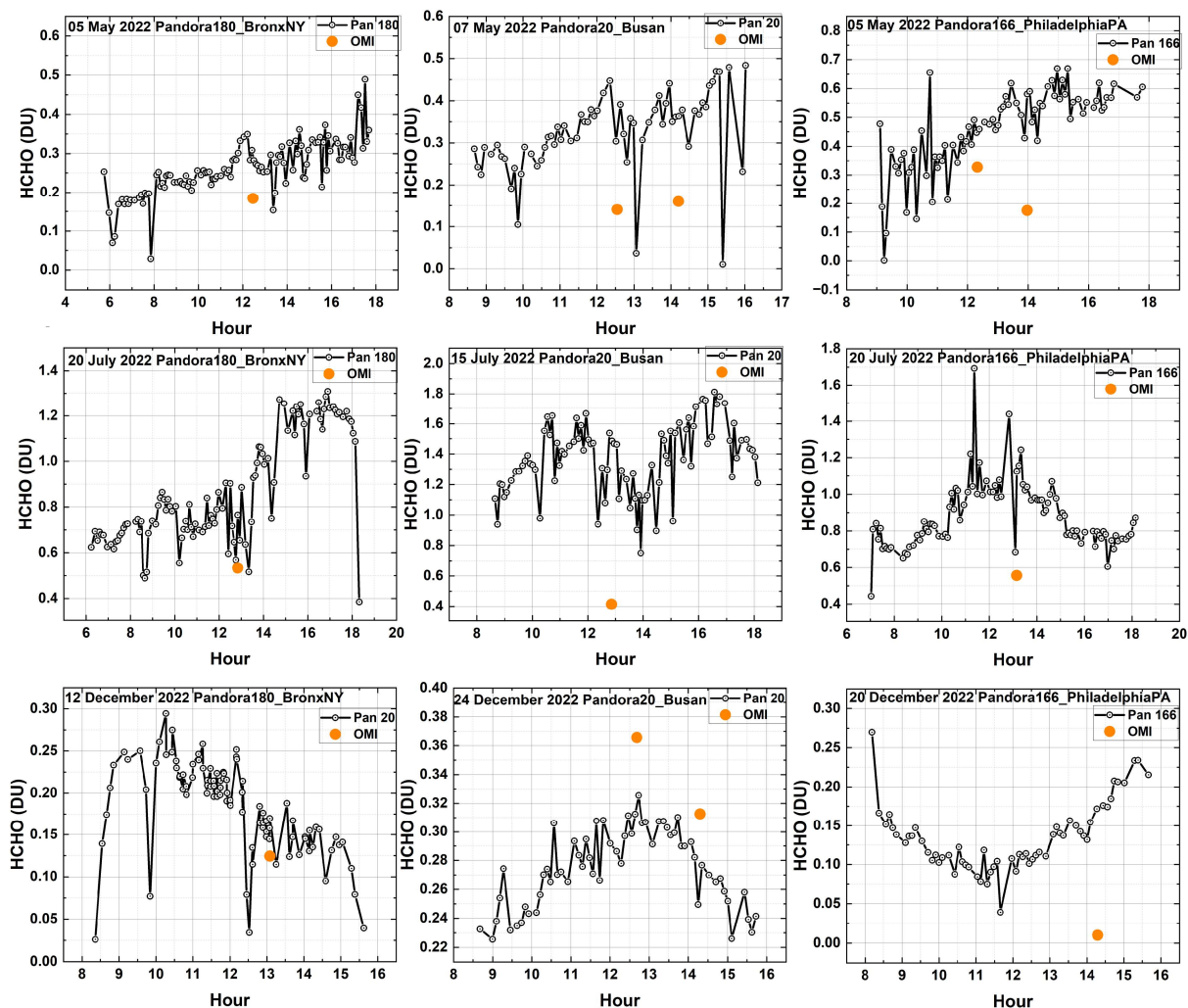


Fig. 09 A comparison between Pandora and OMI (orange circle) total column HCHO. The Local principal investigator for Pan 180 and Pan 166 is Dr. Luke Valin and for Pan 20 is Dr. Jae Hwan Kim.

254

255 Figure 9 illustrates the comparison of TCHCHO retrievals from Pandora and OMI. The spectral fitting
 256 algorithm for detecting HCHO absorption is in the same short wavelength UV spectral region as used for
 257 ozone retrieval, 300 – 360 nm (Gratien et al. 2007). This means that the retrieval sensitivity for “seeing”
 258 all the way to the surface is reduced because of ozone absorption and Rayleigh scattering. Also, small
 259 errors in ozone retrieval can affect the detection of HCHO. This problem is not present for the spectral
 260 fitting of NO₂, since that usually occurs in the visible range 410 – 450 nm where there is only
 261 interference from a weak and narrow water vapor line.

262 Pandora TCHCHO daily average data (Fig. 10) for University of Toronto in Toronto-Scarborough (Lat =
 263 43.784°N , Lon = -79.187°W) shows clear peaks in the summer from the vegetation in a surrounding park
 264 area whereas TCNO₂ shows only small seasonal variation with small peaks also occurring in the summer
 265 for values less than 0.4 DU. Higher values do not show any seasonal variation. The University of Toronto
 266 is located near a major highway, which is a strong source of NO₂ from automobiles and trucks. Unlike
 267 many sites, OMI TCHCHO data over Toronto East (centered on 43.74°N , -79.27°E is about 8 km from the
 268 Pandora site) also shows sporadic summer peak values that are higher than the Pandora 13:00-14:00
 269 averages and all of the Pandora data (Fig. 11).

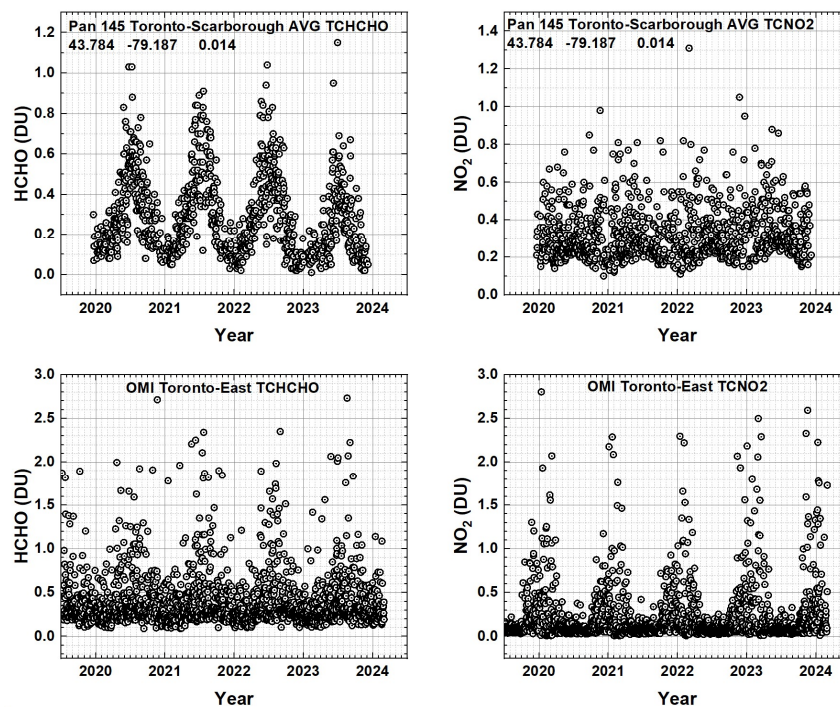


Fig. 10 A comparison of Pandora TCHCHO and TCNO₂ daily average total column amounts for Toronto-Scarborough University of Toronto and OMI data for Toronto East (43.740°N , -79.270°W at approximately $13:20 \pm 0:20$ Local Sun Time, GMT + Longitude/15). The local principal investigator for Pan 145 is Dr. Vitali Fioletov.

270
 271 Using the daily average Pandora data over Toronto-Scarborough (Fig. 10 upper right) shows no visible
 272 hint of an TCNO₂ annual cycle that peaks in winter while the OMI TCNO₂ amounts at 13:40 show a clear
 273 peak in December – January corresponding to the peak winter heating for the city (Figs. 10 lower right).
 274 Instead of the daily average data, using the average TCNO₂ from 13:00 to 14:00 to correspond to the
 275 OMI overpass time and then applying a Lowess(3 month) low-pass filter (Fig. 11) shows less TCNO₂ and a
 276 weaker annual cycle that corresponds to the annual cycle observed by OMI. The OMI FOV includes the
 277 city of Toronto.

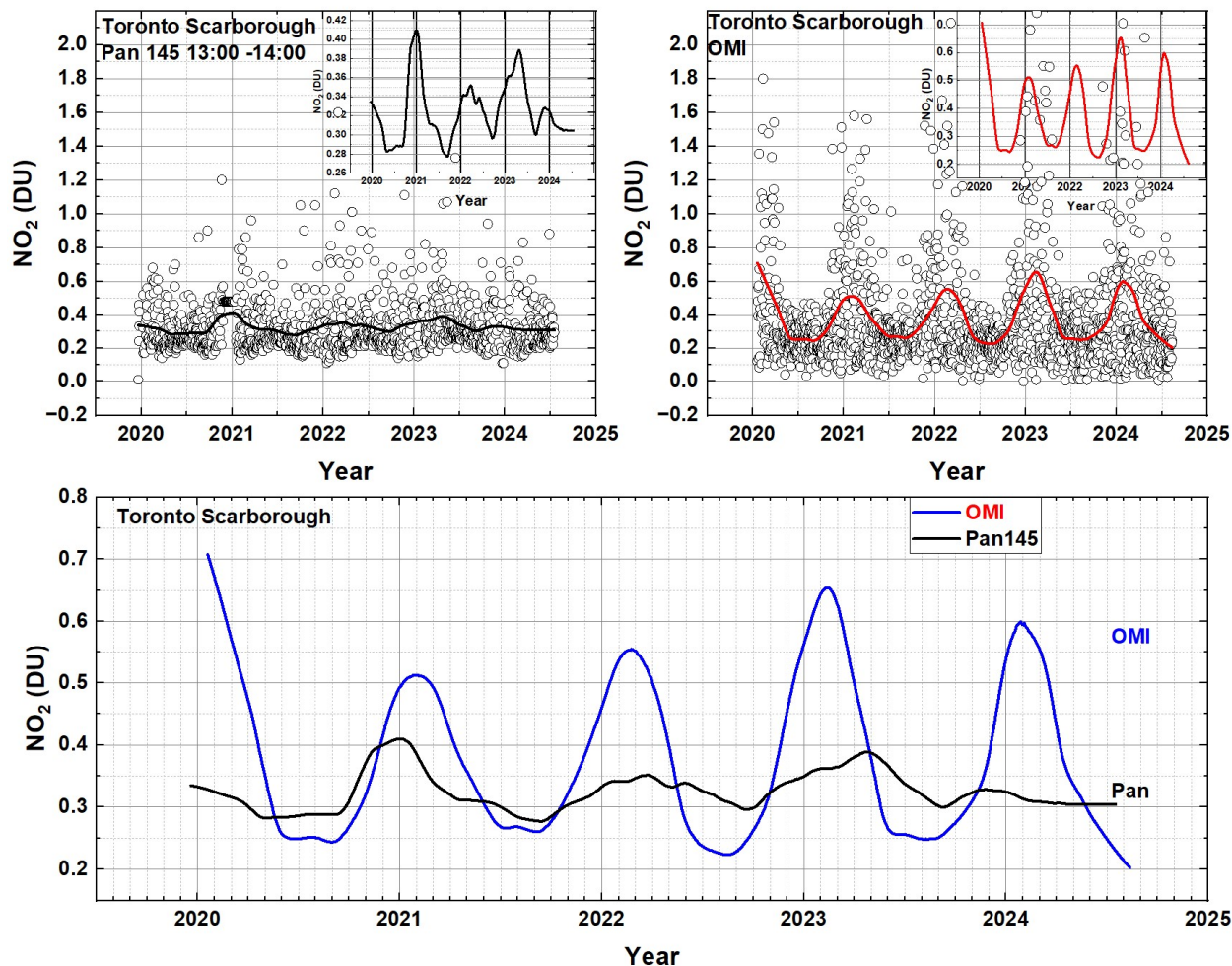


Fig. 11 TCNO₂ annual cycle for Toronto Scarborough from Pan 145 average between 13:00 and 14:00 and OMI. The smooth curves are Lowess(6 Months).

278

279 The lower panel in Fig. 11 reproduces the inset values showing the OMI has a stronger TCNO₂ annual
 280 cycle because it includes the city area of Toronto. Pandora 145 picks up a small amount of the seasonal
 281 signal from Toronto.

282 As shown in Fig. 12, the TCHCHO low-pass filtered time series (2021 – 2024), Lowess(3-months),
 283 measured by OMI and Pandora frequently do not agree. An example is the comparison over Bronx, NY
 284 (Lat = 40.868° Lon = -73.878°) where the Pandora 180 is located in a park with a small lake, while OMI
 285 gridded data is averaged over a large area 33 x 33 km² in New York City with little vegetation.

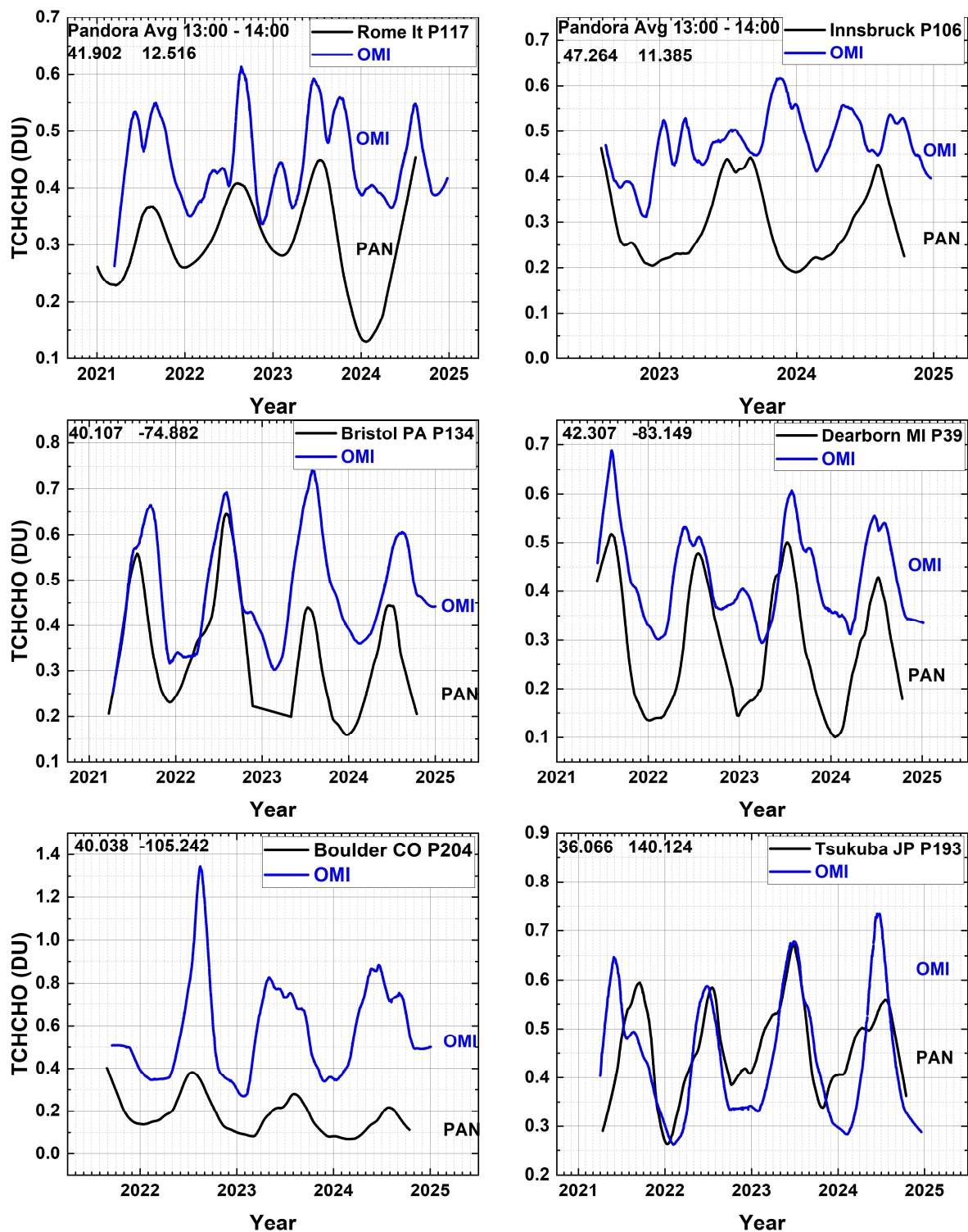


Fig. 12 A comparison between low-pass filtered, Lowess(3 months), OMI and Pandora at six sites with varying degrees of agreement with $TCHCHO(PAN) < TCHCHO(OMI)$. The Local Principal Investigators are P106 Dr. Stefano Casadio, Dr. Kei Shiomi P193, Dr. Alexander Cede P204, Dr. Lukas Valin P39; P134, and Dr. Martin Tiefengraber P106. Latitudes and longitudes are in each upper left corner.

287 The disagreement over Boulder Colorado may be caused by OMI's large field of view that includes lower
 288 altitude grasslands. Similarly, the Innsbruck Pandora is located in a valley at the University of Innsbruck
 289 surrounded by mountain areas where TCHCHO varies over the OMI FOV. Except for a few cases (e.g.,
 290 Bronx, NY and Innsbruck, Austria) OMI and Pandora see the same TCHCHO annual cycle.

291 2.2 Total Ozone Column

292 The retrieval of total column ozone amounts TCO (Figs. 13) serves as a check on the calibration of both
 293 OMI and Pandora that is also needed for spectrally overlapping TCHCHO retrievals. Comparisons of
 294 Pandora TCO with TCO measured by OMI show good agreement suggesting both instruments are well
 295 calibrated in the UV range also needed for retrieving TCHCHO. The good TCO agreement is partly
 296 because most of the O_3 is in the stratosphere near 25 km and the fact that ozone is slowly changing
 297 spatially over the OMI field of regard for the overpass data. Figure 13 shows an example obtained over
 298 Washington DC from the roof of the NASA Headquarters building and from the roof of a building at
 299 Pusan University, Korea. The other sites in Table 1 show similar good monthly average agreement.

300

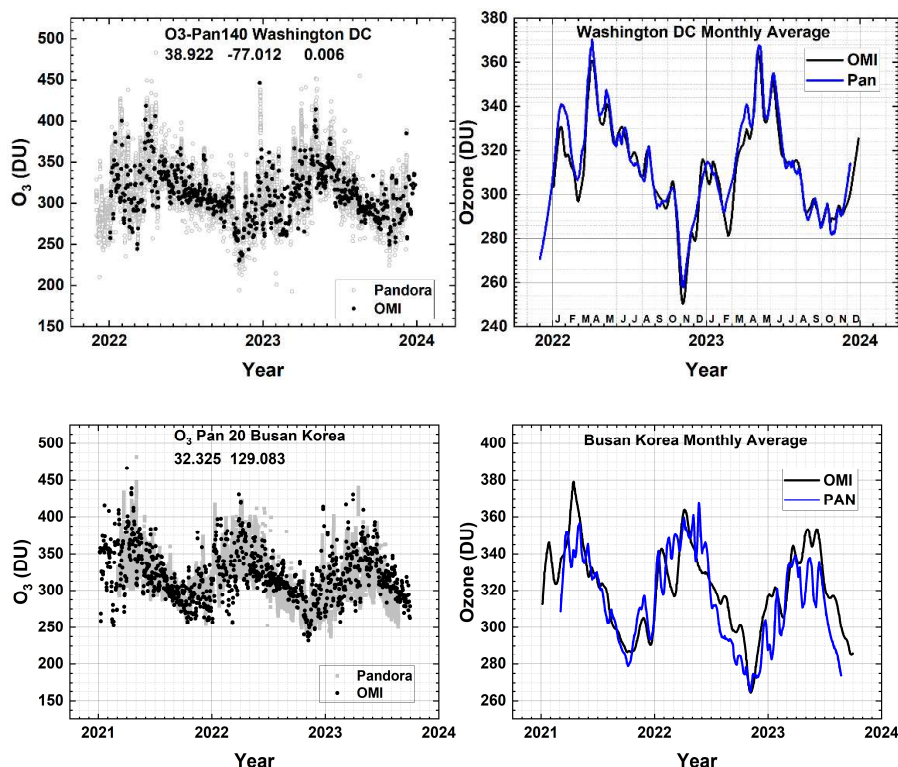


Fig. 13 A comparison of OMI Total Column Ozone values with those obtained from Pandora 140 over the Washington DC site at 38.922°N and -77.012°W and with those obtained from Pandora 20 over the Busan, Korea site at 32.325°N and 129.083°E . The smooth curves (right panel) are Lowess(6-month) fits to data in the left panel. The local principal investigator for Pan 140 is Dr. Jim Szykman and for Pan20 is Jae Hwan Kim.

301

302

303 A test of Pandora UV data is a comparison between EPIC, OMI and Pandora TCO at the specific OMI and
 304 EPIC overpass times (Fig. 14 and 15). that shows good agreement within 1 to 3 %. OMI TCO overpass
 305 data for all Pandora sites and more are available from
 306 <https://avdc.gsfc.nasa.gov/pub/data/satellite/Aura/OMI/V03/L2OVP/OMTO3/>

307 There is also good agreement between daily OMI TCO with that obtained from Pandora (Fig. 14) at most
 308 sites. The values obtained at Granada differ by about 8 DU or 2.9 %.

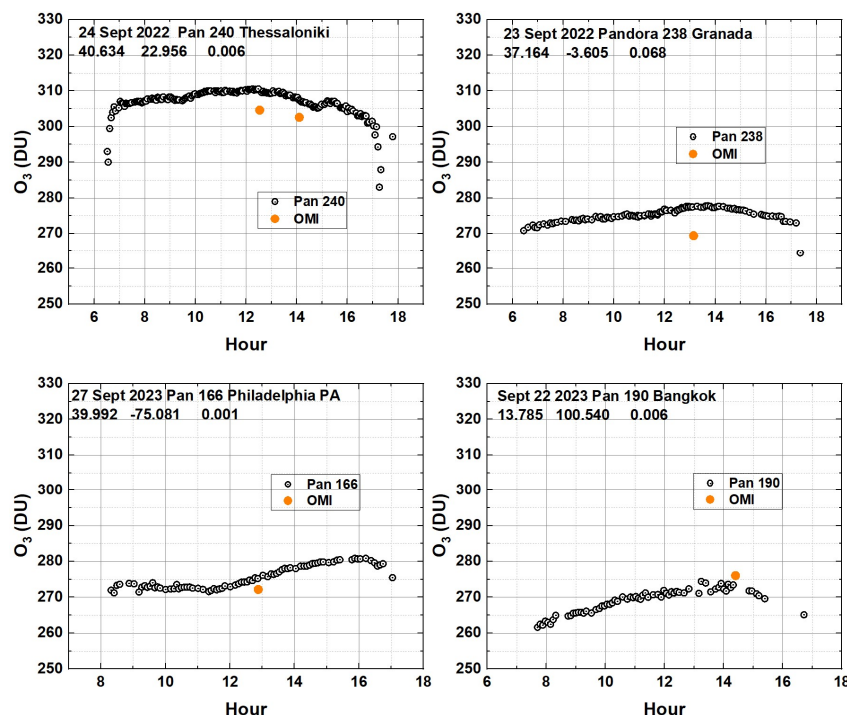


Fig. 14 A comparison of Pandora and OMI retrievals of total column O_3 at the time of the OMI satellite overpass. Local Principal Investigators: Pan 240 Alexander Cede, Pan 238 Inmaculada Foyo Moreno, Pan 166 Lukas Valin, and Pan 190 Surassawadee Phoompan.

The diurnal variation of TCO seen by Pandora can be compared (Fig. 15) with that observed by the Earth Polychromatic Imaging Camera (EPIC) on the DSCOVR (Deep Space Climate Observatory) satellite orbiting about the Earth-Sun gravitational balance Lagrange-1 point (Herman et al., 2018). EPIC obtains simultaneous data from sunrise to sunset once per hour (once per 90 minutes during Northern Hemisphere winter) as the Earth rotates in EPIC's FOV (field of view). Examples of EPIC's view of the whole illuminated Earth are available from <https://epic.gsfc.nasa.gov/>. The spatial resolution for TCO is $18 \times 18 \text{ km}^2$ at the center of the image (the color images have $10 \times 10 \text{ km}^2$ resolution). Retrievals earlier than 07:00 and after 17:00 are not reliable for EPIC or Pandora because of high solar zenith angle effects (spherical geometry effects for $\text{SZA} > 75^\circ$) not included in the retrieval algorithms. In the case of EPIC, this is compounded by high View Zenith Angles VZA outside of 07:00 to 17:00 local sun time.

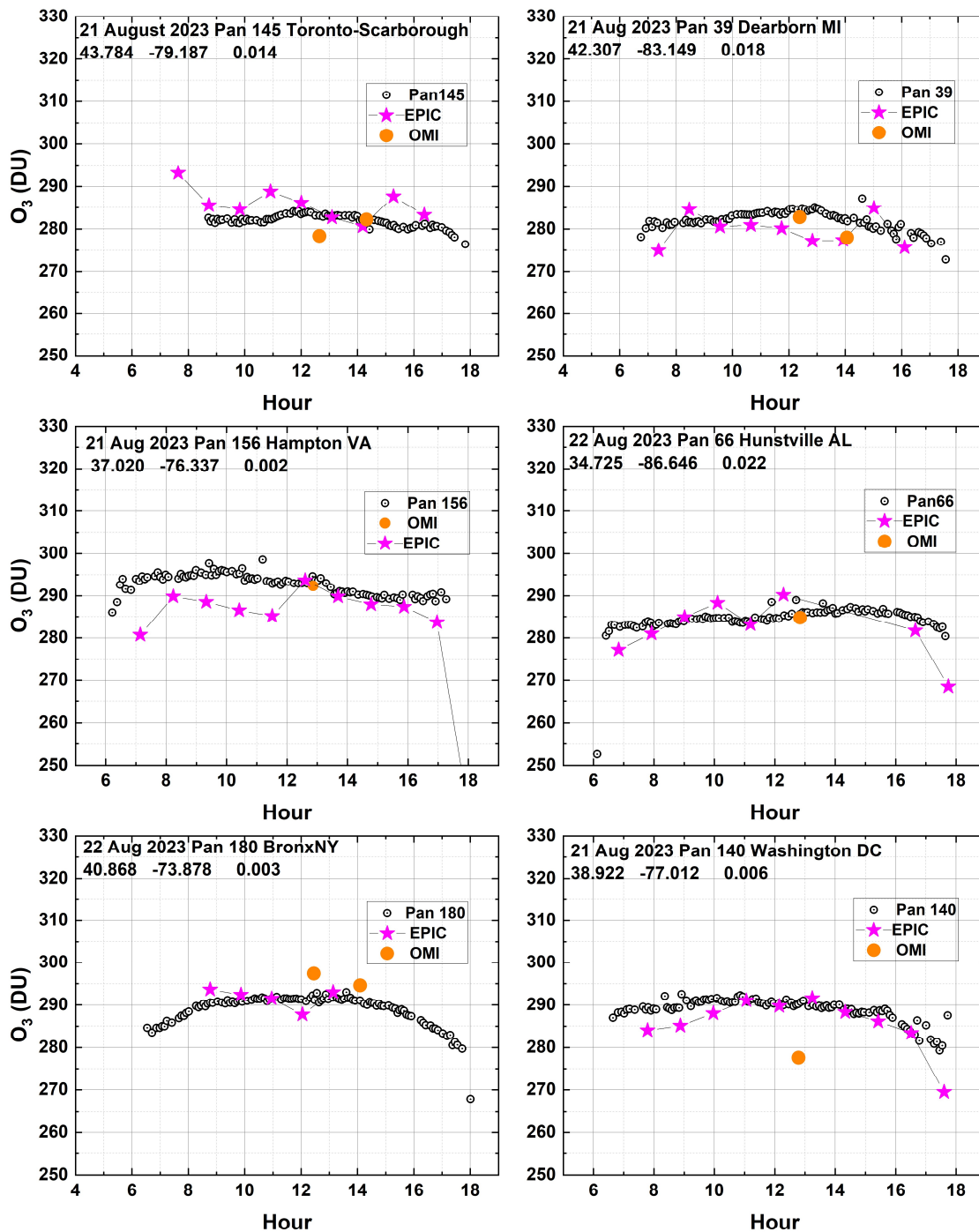


Fig. 15 A comparison of Pandora (Open Circles), EPIC (magenta stars), and OMI (orange circles) retrievals of total column O_3 at the times of the satellite overpasses. Latitude, longitude, and altitude (km) are in the upper left corner. Local Principal Investigators: Pan 145 Vitali Fioletov, Pan 66 Lukas Valin, Pan 39 Lukas Valin, Pan 156 Alexander Cede, Pan 66 Nader Abuhassan, Pan180 Lukas Valin, and Pan 140 Jim Szykman

310 For the cases shown, the TCO data are properly retrieved between 07:00 and 17:00 local solar time. The
311 10:20 and 11:30 EPIC value for Hampton, VA of 286.5 and 285DU differs from Pandora by -3 %. Other
312 differences are smaller. Occasionally, OMI differs from Pandora values as is the case, -4.6 %, for 21
313 August 2023 over Washington, DC.

314 **3.0 Summary**

315 Typical examples of the seasonal variability of HCHO, NO₂, and O₃ in terms of their measured total
316 column TCHCHO, TCNO₂, and TCO have been presented from both ground-based Pandora Spectrometer
317 instruments and the OMI satellite spectrometer instrument overpass retrievals for selected Pandora
318 sites. For most sites, OMI observes the strong seasonal variation of TCHCHO that is also clearly seen in
319 the Pandora data and in surface measurements (Wang et al., 2022). OMI TCHCHO retrievals are usually
320 larger than those retrieved by Pandora but not always (Fig. A2). The amount of seasonal variation for
321 TCHCHO varies depending on the site. For most midlatitude sites, the seasonal variation is significant
322 with peak values occurring during the summer.
323

324 A comparison between the multi-year time series of Pandora and OMI TCNO₂ in urban areas shows that
325 OMI is underestimating the degree of atmospheric NO₂ pollution. The results for TCNO₂ and TCO agree
326 with Pandora data, 2012 – 2017, from a previous study before the Pandora upgrade (Herman et al.,
327 2019). When Pandora is limited to an average of data obtained between 13:00 and 14:00 hours, the
328 agreement between Pandora and OMI TCNO₂ is better. Comparisons of Pandora daily diurnal time
329 series of TCHCHO and TCNO₂ with OMI overpass values show agreement about 30% and 50 % of the
330 time, respectively.

331 OMI TCNO₂ at one shown site, Toronto-Scarborough, shows seasonal variability that the Pandora 145
332 does not appear to see. However, limiting the data to the OMI overpass time between 13:00 and 14:00
333 and applying a Lowess(3-months) low-pass filter reveals a weak annual cycle compared to OMI. This
334 could be because OMI detects the NO₂ source from winter heating in the city, while the Pandora site
335 (University of Toronto campus) is fairly remote from Toronto city buildings and is mostly affected by road
336 traffic as the source of NO₂. The same low-pass filter technique applied to other sites (e.g., Bronx, NY,
337 Busan, Korea, Philadelphia, Pennsylvania, and Boulder, Colorado) also show an annual cycle
338 corresponding to winter heating based on combustion.

339 Total column ozone agrees well in both seasonal variation and in comparison with Pandora at the OMI
340 overpass time. Given the nature of the ozone retrieval algorithm, the good agreement with TCO suggests
341 that the UV calibrations for the Pandoras and OMI are correct. At most well-calibrated Pandora sites,
342 there is good agreement between Pandora TCO with the hourly TCO obtained from the DSCOVR-EPIC
343 instrument observing the Earth from an orbit about the Earth-Sun gravitational balance Lagrange-1
344 point.

345

346

347

348

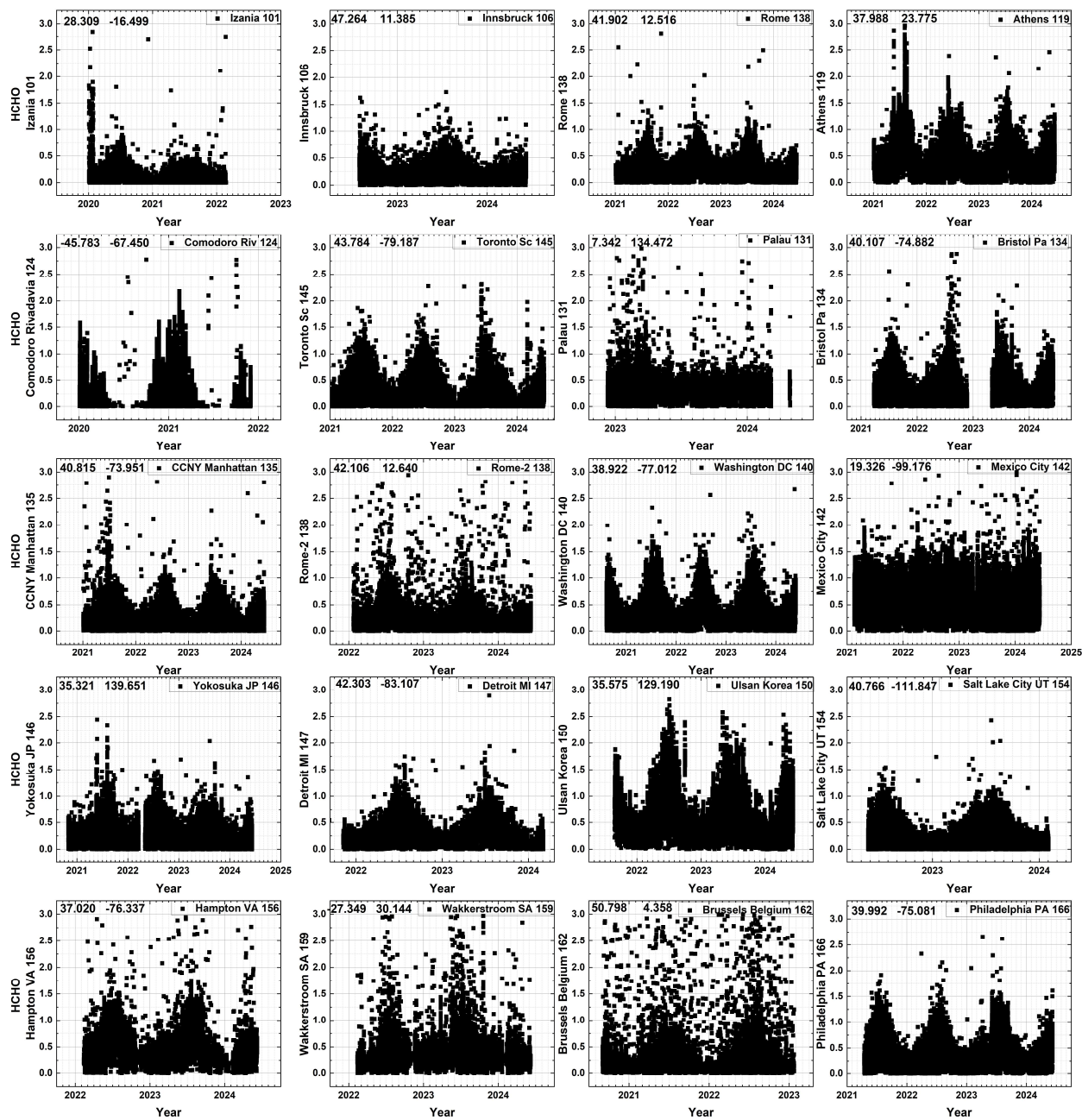


Fig. A1 The seasonal cycle of TCHCHO in DU from 20 randomly selected Pandora TCHCHO time series. The numbers in the upper left corner are the latitude and longitude in degrees and the Pandora instrument number in the right corner.

351

352 Figure A1 shows the seasonal dependence of TCHCHO with the majority of sites showing a maximum
353 TCHCHO in mid-summer.

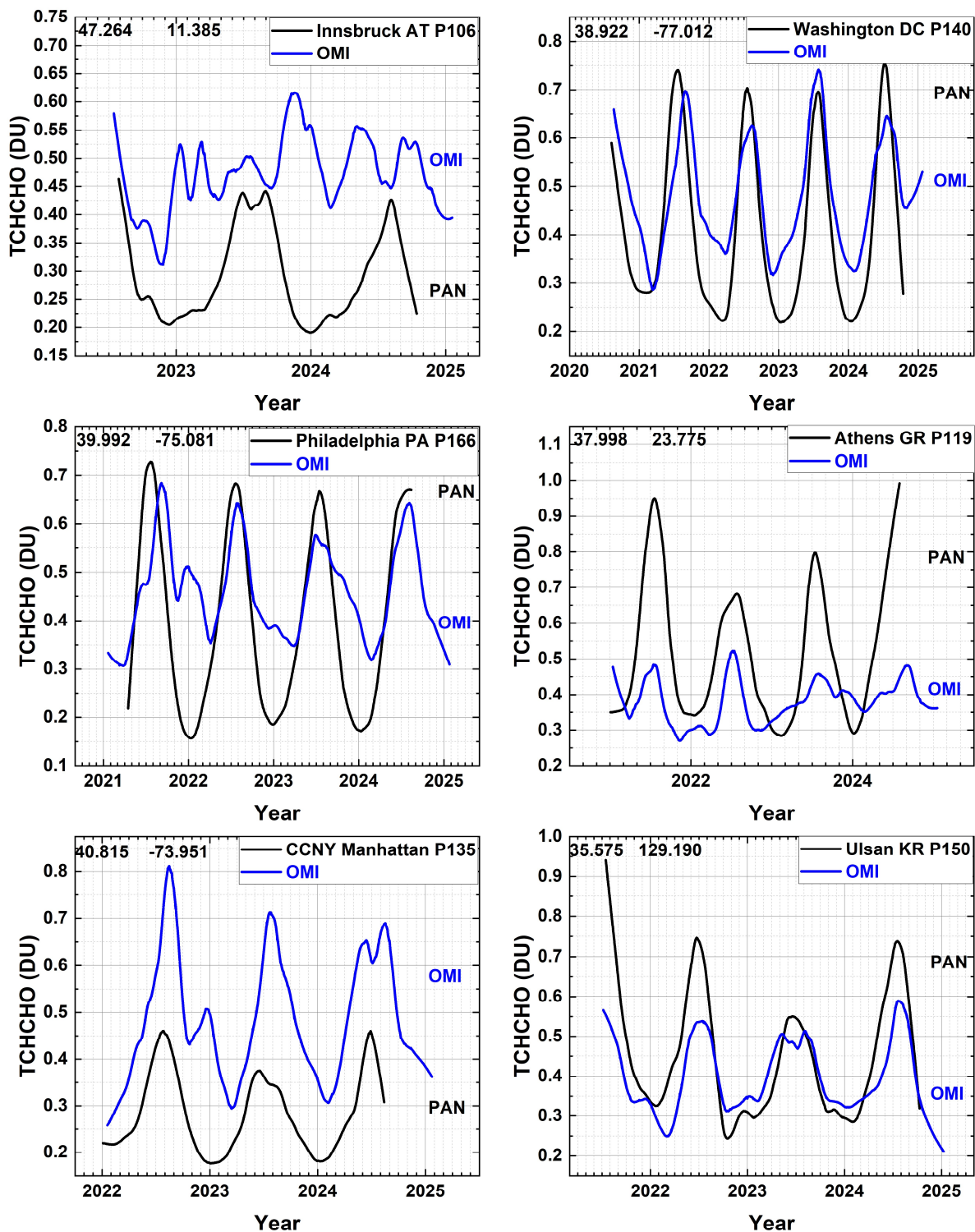


Figure A2 Six cases from Fig. A1 that have significant seasonal variation in TCHCHO. The numbers in the upper left corner are the latitude and longitude in degrees and the Pandora instrument number in the right corner. Principal Investigators are: P106 Dr. Martin Tiefengraber, P140 Dr. Jim Szykman, P166 Dr. Lucas Valin, P119 Dr. Stelios Kazadsi, P135, Dr. Maria Tzortziou, and P150 Dr. Chang Keun Song.

354

355 Figure A2 shows additional cases where OMI and Pandora see the same seasonal dependence but differ
356 on the amount of TCHCHO retrieved.

357 4.0 References

358 Boeke NL, Marshall JD, Alvarez S, Chance KV, Fried A, Kurosu TP, Rappenglück B, Richter D, Walega J,
359 Weibring P, Millet DB. Formaldehyde columns from the Ozone Monitoring Instrument: Urban versus
360 background levels and evaluation using aircraft data and a global model, *J. Geophys. Res.* 2011 Mar
361 16;116(D5):10.1029/2010jd014870, doi: 10.1029/2010jd014870, 2011.

362

363 Boersma, Klaas & Jacob, D. & Trainic, Miri & Rudich, Yinon & De Smedt, Isabelle & R, Dirksen & Eskes,
364 Henk, Validation of urban NO₂ concentrations and their diurnal and seasonal variations observed from
365 space (SCIAMACHY and OMI sensors) using in situ measurements in Israeli cities. *Atmos Chem Phys*, 9,
366 10.5194/acp-9-3867-2009, 2009.

367

368 Cleveland, W. S.: Robust Locally Weighted Regression and Smoothing Scatterplots, *J. Am. Stat. Assoc.*, 74,
369 829–836, <https://doi.org/10.2307/2286407>, 1979.

370

371 Cleveland, W. S. and Devlin, S. J.: Locally Weighted Regression: An Approach to Regression Analysis by
372 Local Fitting, *J. Am. Stat. Assoc.*, 83, 596–610, <https://doi.org/10.1080/01621459.1988.10478639>, 1988.

373

374 Faustini, Annunziata and Rapp, Regula and Forastiere, Francesco, Nitrogen dioxide and mortality: review
375 and meta-analysis of long-term studies, *European Respiratory Journal*, 44, 744–753,
376 <https://doi.org/10.1183/09031936.00114713>, 2014.

377

378 Gratien, A., B. Picquet-Varrault, J. Orphal, E. Perraudin, J.-F. Doussin and J.-M. Flaud, Laboratory
379 intercomparison of the formaldehyde absorption cross sections in the infrared (1660–1820 cm⁻¹ and
380 ultraviolet (300–360 nm) spectral regions, *J. Geophys. Res.*, **112**, <https://doi.org/10.1029/2006JD007201>,
381 D05305 1-10, 2007.

382

383 Herman, J., A. Cede, E. Spinei, G. Mount, M. Tzortziou, and N. Abuhassan, NO₂ column amounts from
384 ground-based Pandora and MFDOAS spectrometers using the direct-sun DOAS technique:
385 Intercomparisons and application to OMI validation, *J. Geophys. Res.*, 114, D13307,
386 doi:[10.1029/2009JD011848](https://doi.org/10.1029/2009JD011848), 2009.

387

388 Herman, J., Huang, L., McPeters, R., Ziemke, J., Cede, A., and Blank, K.: Synoptic ozone, cloud reflectivity,
389 and erythemal irradiance from sunrise to sunset for the whole earth as viewed by the DSCOVR
390 spacecraft from the earth sun Lagrange 1 orbit, *Atmos. Meas. Tech.*, 11, 177–194,
391 <https://doi.org/10.5194/amt-11-177-2018>, 2018.

392

393 Herman, J., Abuhassan, N., Kim, J., Kim, J., Dubey, M., Raponi, M., and Tzortziou, M.: Underestimation of
394 column NO₂ amounts from the OMI satellite compared to diurnally varying ground-based retrievals from
395 multiple PANDORA spectrometer instruments, *Atmos. Meas. Tech.*, 12, 5593–5612,
396 <https://doi.org/10.5194/amt-12-5593-2019>, 2019.

397

- 398 Kim, K. H., Jahan, S. A., & Lee, J. T., Exposure to Formaldehyde and Its Potential Human Health
399 Hazards. *Journal of Environmental Science and Health, Part C*, 29(4), 277–299.
400 <https://doi.org/10.1080/10590501.2011.629972>, 2011.
401
- 402 Lamsal, L. N., Krotkov, N. A., Celarier, E. A., Swartz, W. H., Pickering, K. E., Bucsela, E. J., Gleason, J. F.,
403 Martin, R. V., Philip, S., Irie, H., Cede, A., Herman, J., Weinheimer, A., Szykman, J. J., and Knepp, T. N.:
404 Evaluation of OMI operational standard NO₂ column retrievals using in situ and surface-based NO₂
405 observations, *Atmos. Chem. Phys.*, 14, 11587–11609, <https://doi.org/10.5194/acp-14-11587-2014>,
406 2014.
407
- 408 Lamsal, L., Duncan, Bryan, Yoshida, Yasuko, Krotkov, Nickolay, Pickering, Kenneth, Streets, David, Lu,
409 Zifeng, U.S. NO₂ trends (2005–2013): EPA Air Quality System (AQS) data versus improved observations
410 from the Ozone Monitoring Instrument (OMI). *Atmospheric Environment*. 110.
411 10.1016/j.atmosenv.2015.03.055, 2015.
412
- 413 Levelt, P. F., Joiner, J., Tamminen, J., Veefkind, J. P., Bhartia, P. K., Stein Zweers, D. C., Duncan, B. N.,
414 Streets, D. G., Eskes, H., van der A, R., McLinden, C., Fioletov, V., Carn, S., de Laat, J., DeLand, M.,
415 Marchenko, S., McPeters, R., Ziemke, J., Fu, D., Liu, X., Pickering, K., Apituley, A., González Abad, G.,
416 Arola, A., Boersma, F., Chan Miller, C., Chance, K., de Graaf, M., Hakkarainen, J., Hassinen, S., Ialongo, I.,
417 Kleipool, Q., Krotkov, N., Li, C., Lamsal, L., Newman, P., Nowlan, C., Suleiman, R., Tilstra, L. G., Torres, O.,
418 Wang, H., and Wargan, K.: The Ozone Monitoring Instrument: overview of 14 years in space, *Atmos.*
419 *Chem. Phys.*, 18, 5699–5745, <https://doi.org/10.5194/acp-18-5699-2018>, 2018.
420 Morfopoulos C, Müller J-F, Stavrakou T, et al. Vegetation responses to climate extremes recorded by
421 remotely sensed atmospheric formaldehyde. *Glob Change Biol.*, 28, 1809–1822.
422 <https://doi.org/10.1111/gcb.15880>, 2021.
423
- 424 Newmark, G. (2001). Emissions Inventory Analysis of Mobile Source Air Pollution In Tel Aviv, Israel,
425 *Transportation Research Record*, Vol. 1750, p. 40-48, <https://doi.org/10.3141/1750-0>, 2001.
- 426 Nussbaumer, C. M., Crowley, J. N., Schuladen, J., Williams, J., Hafermann, S., Reiffs, A., Axinte, R.,
427 Harder, H., Ernest, C., Novelli, A., Sala, K., Martinez, M., Mallik, C., Tomsche, L., Plass-Dülmer, C., Bohn,
428 B., Lelieveld, J., and Fischer, H.: Measurement report: Photochemical production and loss rates of
429 formaldehyde and ozone across Europe, *Atmos. Chem. Phys.*, 21, 18413–18432,
430 <https://doi.org/10.5194/acp-21-18413-2021>, 2021.
- 431 Peng, W.-X., X.-C. Yue, H.-L. Chen, N.L. Ma, Z. Quan, Q. Yu, C. Sonne, A review of plants formaldehyde
432 metabolism: Implications for hazardous emissions and phytoremediation, *J. Hazard. Mater.* 436 Article
433 129304, <https://doi.org/10.1016/j.jhazmat.2022.129304>, 2022.
- 434 Spinei, E., Whitehill, A., Fried, A., Tiefengraber, M., Knepp, T. N., Herndon, S., Herman, J. R., Müller, M.,
435 Abuhassan, N., Cede, A., Richter, D., Walega, J., Crawford, J., Szykman, J., Valin, L., Williams, D. J., Long,
436 R., Swap, R. J., Lee, Y., Nowak, N., and Poche, B.: The first evaluation of formaldehyde column
437 observations by improved Pandora spectrometers during the KORUS-AQ field study, *Atmos. Meas. Tech.*,
438 11, 4943–4961, <https://doi.org/10.5194/amt-11-4943-2018>, 2018.
- 439 Spinei, E., Tiefengraber, M., Müller, M., Gebetsberger, M., Cede, A., Valin, L., Szykman, J., Whitehill, A.,
440 Kotsakis, A., Santos, F., Abuhassan, N., Zhao, X., Fioletov, V., Lee, S. C., and Swap, R.: Effect of
441 polyoxymethylene (POM-H Delrin) off-gassing within the Pandora head sensor on direct-sun and multi-

- 442 axis formaldehyde column measurements in 2016–2019, *Atmos. Meas. Tech.*, 14, 647–663,
443 <https://doi.org/10.5194/amt-14-647-2021>, 2021.
- 444 Stavrakou, T., Müller, J.-F., Bauwens, M., Boersma, K. F. & van Geffen, J. Satellite evidence for changes in
445 the NO₂ weekly cycle over large cities. *Sci. Rep.* <https://doi.org/10.1038/s41598-020-66891-0> (2020).
- 446 Tzortziou, M., Herman, J.R., Cede, A. *et al.* Spatial and temporal variability of ozone and nitrogen dioxide
447 over a major urban estuarine ecosystem. *J Atmos Chem* **72**, 287–309, [https://doi.org/10.1007/s10874-](https://doi.org/10.1007/s10874-013-9255-8)
448 [013-9255-8](https://doi.org/10.1007/s10874-013-9255-8), 2015.
- 449 Van der A, R. J., H. J. Eskes, K. F. Boersma, T. P. C. van Noije, M. Van Roozendaal, I. De Smedt, D. H. M. U.
450 Peters, and E. W. Meijer, Trends, seasonal variability and dominant NO_x source derived from a ten year
451 record of NO₂ measured from space, *J. Geophys. Res.*, 113, D04302, doi:10.1029/2007JD009021, 2008.
- 452 Wang, P.; Holloway, T.; Bindl, M.; Harkey, M.; De Smedt, I. Ambient Formaldehyde over the United
453 States from Ground-Based (AQS) and Satellite (OMI) Observations. *Remote Sens.* 14, 2191,
454 <https://doi.org/10.3390/rs14092191>, 2022.
- 455 Wittrock, F., Richter, A., Oetjen, H., Burrows, Wittrock, F., Richter, A., Oetjen, H., Burrows, J.P., Kanakidou,
456 Myriokefalitakis, S., Volkamer, R., Beirle, S., Platt, U., and Wagner, T.: Simultaneous global observations of
457 glyoxal and formaldehyde from space, *Geophys. Res. Lett.*, 33, L16804,
458 <https://doi.org/10.1029/2006GL026310>, 2006.
- 459 Zhang, Y., Li, R., Min, Q., Bo, H., Fu, Y., Wang, Y., & Gao, Z. (2019). The controlling factors of atmospheric
460 formaldehyde (HCHO) in Amazon as seen from satellite. *Earth and Space Science*, 6, 959–971.
461 <https://doi.org/10.1029/2019EA000627>, 2019.
- 462

463 **Author contribution:**

464 Jay Herman is responsible for writing the paper and creating the figures. Jianping Mao obtained the
465 EPIC overpass data for the Pandora sites and discussed aspects of the paper.

466 **Data Availability**

467 Worldwide Pandora data for 63 sites is available from the Austrian Pandonia project website
468 <https://data.pandonia-global-network.org/> or from a NASA backup site updated every week.

469 https://avdc.gsfc.nasa.gov/pub/DSCOVR/Pandora/DATA_02/

470 The OMI overpass TCHCHO and TCNO2 data are found at

471 <https://avdc.gsfc.nasa.gov/pub/data/satellite/Aura/OMI/V03/L2OVP/OMHCHO/>.

472 <https://avdc.gsfc.nasa.gov/pub/data/satellite/Aura/OMI/V03/L2OVP/OMNO2/>

473 OMI TCO overpass data are available from

474 <https://avdc.gsfc.nasa.gov/pub/data/satellite/Aura/OMI/V03/L2OVP/OMTO3/>

475

476 **Competing interests:**

477 The authors declares that they have no conflicts of interest.

478

479 Funding: This study is funded by the DSCOVR-EPIC project through the University of Maryland
480 Baltimore County

481

482 **Acknowledgements:**

483 The authors want to acknowledge the contribution of each of the Pandora Principal Investigators
484 included in the figure captions and for the OMI team and Dr. Lok Lamsal for making OMI overpass
485 data available. Acknowledgement is also due to the Pandonia team lead by Dr. Alexander Cede for
486 processing all of the Pandora data and devising the retrieval algorithms and to Dr. Nader Abuhassan
487 for building and calibrating all of the Pandora spectrometer systems. The Pandonia Global Network
488 PGN is a bilateral project supported with funding from NASA and ESA.

489

490 **Figure Captions**

491 Fig. 1 Seasonal and daily behavior of HCHO and NO₂ from Pan 180 located in the Bronx, NYC at 40.868°N,
 492 -73.878°W. The blue lines are a Lowess(0.033) fit to the data (light grey), which is approximately a 1-
 493 month local least-squares average. The Local principal investigator for Pan 180 is Dr. Luke Valin.

494 Fig. 2 The daily average seasonal variation of HCHO and NO₂ over Fordham University in Bronx, New
 495 York City from Pandora 180 at 40.868° latitude, -73.878° longitude, and 0.003 km altitude. Each point is
 496 a daily average of the data in Fig.1. Local principal investigator: Dr. Luke Valin

497 Fig. 3 The seasonal variation of TCHCHO and TCNO₂ over New Haven Connecticut from Pandora 64 at
 498 41.301°N latitude and -72.903°W longitude. Each point is a daily average. Local principal investigator:
 499 Dr. Nader Abuhassan.

500 Fig. 4 The seasonal variation of TCHCHO and TCNO₂ over equatorial Bangkok Indonesia at 13.785°N and
 501 100.540°E. The local principal investigator is Surassawadee Phoompanit.

502 Fig. 5 Seasonal variation in daily average TCHCHO and TCNO₂ in Tel Aviv Israel from Pandora 182 located
 503 at 32.113°N 34.085°E at a height of 8 meters. The local principal investigator for Pan 182 is Dr. Michal
 504 Rozenhaimer.

505 Fig. 6 Seasonal variation in daily average HCHO and NO₂ in Wakkerstroom South Africa from Pandora
 506 159 located at -27.359°S and 30.144°E. Local principal investigator: B. Scholes

507 Fig. 7 Upper 2 Panels: Comparison of OMI (approximately 13:30) and Pandora (07:00 – 17:00) total
 508 column NO₂ time series in Bronx NY (40.868°N, -73.878°W) and Busan Korea (35.235°N, 129.083°E).
 509 Lower 4 Panels: Pandora data for Bronx, Busan, Philadelphia (39.992°N, -75.081°W) and Boulder
 510 (40.0375°N, -105.242°W) are averaged between 13:00 – 14:00 hours. Both OMI (blue) and Pandora
 511 (black) then have a Lowess(3-month) low-pass filter applied. Local principal investigator for Pan20 is Jae
 512 Hwan Kim, for Pan 180 and Pan 166 is Dr. Luke Valin, and for Pan 204 Dr. Nader Abuhassan.

513 Fig. 8 A comparison between Pandora and OMI (Orange circle) total column NO₂ for 3 locations (Bronx,
 514 New York, Busan Korea, Philadelphia, Pennsylvania). The Local principal investigator for Pan 180 and Pan
 515 166 is Dr. Lukas Valin and for Pan 20 is Dr. Jae Hwan Kim.

516 Fig. 9 A comparison between Pandora and OMI (purple circle) total column HCHO. The Local principal
 517 investigator for Pan 180 is Dr. Luke Valin and for Pan 20 is Dr. Jae Hwan Kim.

518 Fig. 10 A comparison of Pandora TCHCHO and TCNO₂ daily average total column amounts for Toronto-
 519 Scarborough University of Toronto and OMI data for Toronto East (43.740°N, -79.270°W at
 520 approximately 13:20±0:20 Local Sun Time, GMT + Longitude/15). The local principal investigator for Pan
 521 145 is Dr. Vitali Fioletov.

522 Fig. 11 TCNO₂ annual cycle for Toronto Scarborough from Pan 145 average between 13:00 and 14:00
 523 and OMI. The smooth curves are Lowess(6 Months).

Fig. 12 A comparison between low-pass filtered, Lowess(3 months), OMI and Pandora at six sites with

524 varying degrees of agreement with $TCHCHO(\text{Pan}) < TCHCHO(\text{OMI})$. The Local Principal Investigators are
525 P106 Dr. Stefano Casadio, Dr. Kei Shiomi P193, Dr. Alexander Cede P204, Dr. Lukas Valin P39; P134, and
526 Dr. Martin Tiefengraber P106. Latitudes and longitudes are in each upper left corner.

525 Fig. 13 A comparison of OMI Total Column Ozone values with those obtained from Pandora 140 over the
526 Washington DC site at 38.922°N and -77.012°W and with those obtained from Pandora 20 over the
527 Busan, Korea site at 32.325°N and 129.083°E . The smooth curves (right panel) are Lowess(6-month) fits
528 to data in the left panel. The local principal investigator for Pan 140 is Dr. Jim Szykman and for Pan20 is
529 Jae Hwan Kim.

530 Fig. 14 A comparison of Pandora and OMI retrievals of total column O_3 at the time of the OMI satellite
531 overpass. Local Principal Investigators: Pan 240 Alexander Cede, Pan 238 Inmaculada Foyo Moreno, Pan
532 166 Lukas Valin, and Pan 190 Surassawadee Phoompan.

533 Fig. 15 A comparison of Pandora (Open Circles), EPIC (magenta stars), and OMI (orange circles) retrievals
534 of total column O_3 at the times of the satellite overpasses. Local Principal Investigators: Pan 145 Vitali
535 Fioletov, Pan 66 Lukas Valin, Pan 39 Lukas Valin, Pan 156 Alexander Cede, Pan 66 Nader Abuhassan,
536 Pan180 Lukas Valin, and Pan 140 Jim Szykman.

537 Fig. A1 The seasonal cycle of TCHCHO in DU from 20 randomly selected Pandora TCHCHO time series.
538 The numbers in the upper left corner are the latitude and longitude in degrees and the Pandora
539 instrument number in the right corner.

540 Figure A2 shows additional cases where OMI and Pandora see the same seasonal dependence but differ
541 on the amount of TCHCHO retrieved.

542

543 **Author contribution:**

544 Jay Herman is responsible for writing the paper and creating the figures. Jianping Mao obtained the
545 EPIC overpass data for the Pandora sites and discussed aspects of the paper.

546 **Data Availability**

547 Worldwide Pandora data for 63 sites is available from the Austrian Pandonia project website
548 <https://data.pandonia-global-network.org/> or from a NASA backup site updated every week.

549 https://avdc.gsfc.nasa.gov/pub/DSCOVER/Pandora/DATA_02/

550 The OMI overpass TCHCHO and TCNO2 data are found at

551 <https://avdc.gsfc.nasa.gov/pub/data/satellite/Aura/OMI/V03/L2OVP/OMHCHO/>.

552 <https://avdc.gsfc.nasa.gov/pub/data/satellite/Aura/OMI/V03/L2OVP/OMNO2/>

553 OMI TCO overpass data are available from

554 <https://avdc.gsfc.nasa.gov/pub/data/satellite/Aura/OMI/V03/L2OVP/OMTO3/>

555

556 **Competing interests:**

557 The authors declares that they have no conflicts of interest.

558

559 Funding: This study is funded by the DSCOVER-EPIC project through the University Of Maryland
560 Baltimore County

561

562 **Acknowledgements:**

563 The authors want to acknowledge the contribution of each of the Pandora Principal Investigators
564 included in the figure captions and for the OMI team and Dr. Lok Lamsal for making OMI overpass
565 data available. Acknowledgement is also due to the Pandonia team lead by Dr. Alexander Cede for
566 processing all of the Pandora data and devising the retrieval algorithms and to Dr. Nader Abuhassan
567 for building and calibrating all of the Pandora spectrometer systems. The Pandonia Global Network
568 PGN is a bilateral project supported with funding from NASA and ESA.

569